Supporting information for Environ. Sci. Technol. article:

Ball milling synthesized manganese oxide as high active catalyst for gaseous POPs removal: significance of mechanically induced oxygen vacancies

*Yang Yang, Shuzhen Zhang, Siwen Wang, Kunlun Zhang, Haizhu Wang, Jun Huang, Shubo Deng, Bin Wang, Yujue Wang, Gang Yu**

School of Environment, Beijing Key Laboratory for Emerging Organic Contaminants Control, State Key Joint Laboratory of Environment Simulation and Pollution Control (SKLESPC), Tsinghua University, Beijing 100084, China

This seventeen pages material covers two texts, eight figures and three tables.

Text S1 Preparation of OMS-2

A solid mixture composed of $KMnO_4$ (0.5 g) and $MnSO_4 \cdot H_2O$ (0.21 g) was transferred into a Teflon-lined autoclave (100 mL). The autoclave was filled with ultra-pure water (75 mL), and then sealed and kept in an oven at 160 °C for 12 h. After that, the autoclave was cooled to room temperature. The obtained black slurry was filtered, washed and dried at 110 °C for 4 h.

Text S2 Experimental details

X-ray diffraction (XRD) analyses were done on D/MAX-RB (Rigaku) X-ray diffractometer with Cu Kα radiation. Elemental composition was analyzed by inductively coupled plasma atomic emission spectroscopy (ICP-AES, RIS Intrepid II XSP). Surface elements were analyzed by X-ray photoelectron spectroscopy (XPS) conducted on PHI-5300 electron spectrometer. The morphology of catalysts was observed on JSM-7401F field emission scanning electron microscope (FESEM)

Surface area was measured by N_2 adsorption at 77 K on Quantachrome Autosorb iQ gas sorption system. Before the measurements, the sample was outgassed for 4 h at 300 °C. Specific surface area was calculated based on Brunauer-Emmertt-Teller (BET) model. Distribution of pore size was obtained by fitting the adsorption isotherm with non-local density functional theory (NLDFT).[1, 2]

Hydrogen temperature programmed reduction (H_2-TPR), oxygen temperature programmed desorption (O_2-TPD), NH_3 temperature programmed desorption (NH_3-TPD) analyses were conducted on AutoChem II 2920 chemisorption analyzer. Experimental details are described as follows:

H_2-TPR: 50 mg catalyst was heated to 110 °C and purged with He for 1h. After that, a mixture of 5% H_2/Ar (60 cm^3 min^{-1}) was purged into the reaction tube for TPR reaction. The temperature was increased at a rate of 10 °C min^{-1}, and the H_2 consumption was monitored by TCD detector.

O_2-TPD: 100 mg catalyst was heated to 110 °C and purged with He for 1 h to remove surface H_2O and physically adsorbed molecular oxygen. Then the catalyst

was purged with He and heated from 100 to 900 ˚C at a rate of 10 ˚C min. The release of O_2 was monitored using TCD detector.

NH_3-TPD: 20 mg catalysts dispersed in inactive quartz sand was purged with 10 % NH_3/He at 100 °C for 30 min and then continuously purged with He for 30 min. Desorption of NH_3 was carried out from 100 to 400 °C at a heating rate of 10 °C min^{-1} in 60 cm^3 min^{-1} He flow. The final temperature was maintained for 1 h to achieve complete desorption.

For all the analyses, the outlet gas was passed through the cold trap (cooled by mixture of liquid nitrogen and isopropanol) before entering TCD detector to avoid the potential interference of water vapor.

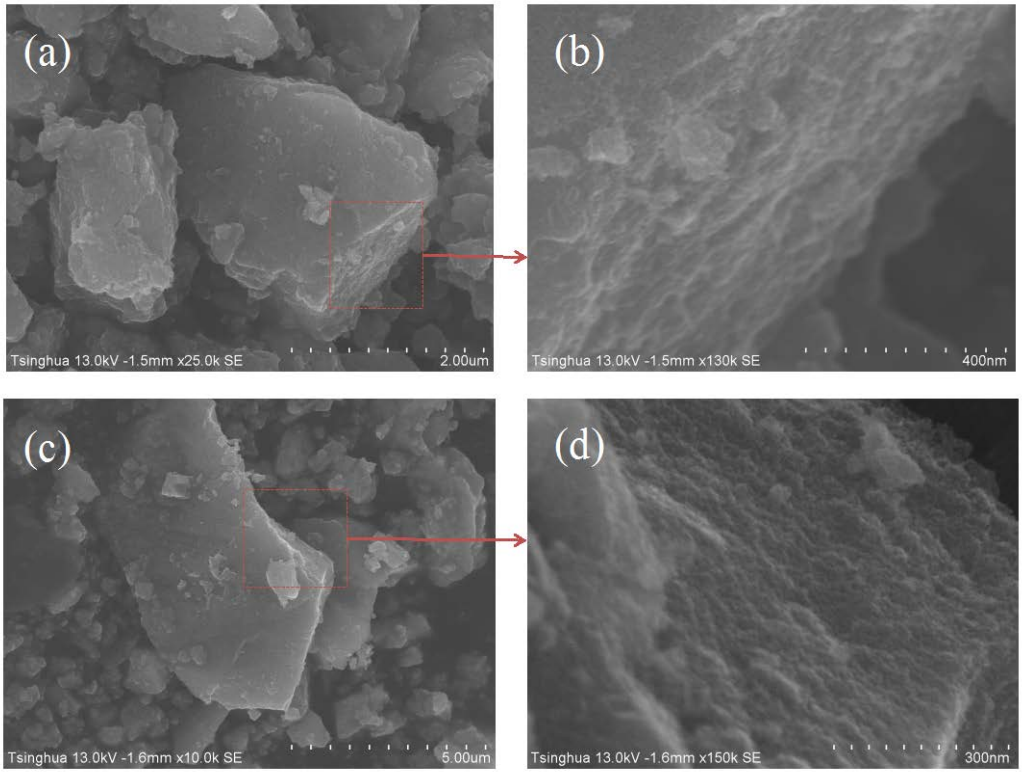

Figure S1. FESEM images of BM0 (a and b) and BM2 (c and d).

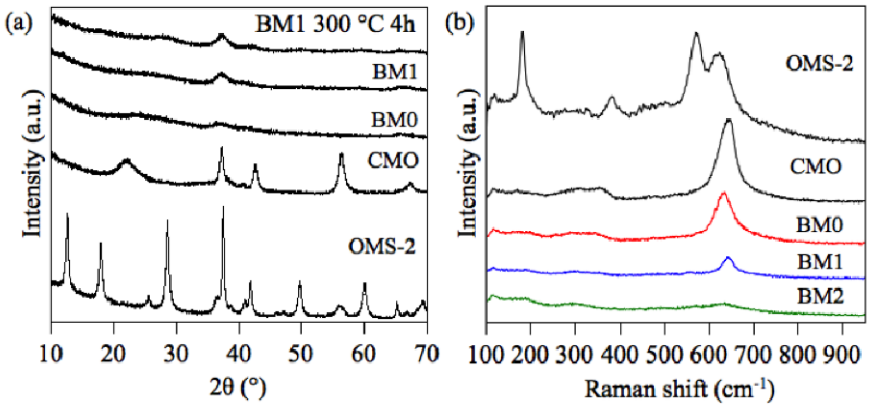

Figure S2. (a) XRD and (b) Raman patterns of samples

The reference catalyst OMS-2 can be well indexed to the cryptomelane-type structure (JCPDS 29-1020). As for CMO diffraction peaks were found at 37, 43, and 57°, indicating the presence of nsutite phase (JCPDS 17-0510). BM0 prepared by top-down approach only show weak and broad peak at 37 °, implying its amorphous structure. The product (BM1) generated from ball milling of KMnO4 and $MnC_4H_6O_4{\cdot}4H_2O$ exhibit amorphous structure, and the structure remain stable after 300 °C calcination for 4h. Similar stability was observed on sample BM2 generated from the reaction between $KMnO_4$ and $MnSO_4{\cdot}H_2O$ (data not shown).

In Raman spectra, the peaks at 181 and 386 cm^{-1} can be ascribed to the deformation modes of Mn-O-Mn, while the peaks at 630 and 578 cm^{-1} can be assigned to the Mn-O vibrations that are orthogonal and along the direction of the MnO_6 octahedral double chains.[3, 4] The well crystalline OM-2 have strong Mn-O-Mn vibration response an perfect MnO_6 octahedral structure. In contrast, disordered Mn-O-Mn bonds and MnO_6 octahedral is observed on CMO. All these Mn-O bonds were further distorted on BM0, BM1, and BM2.

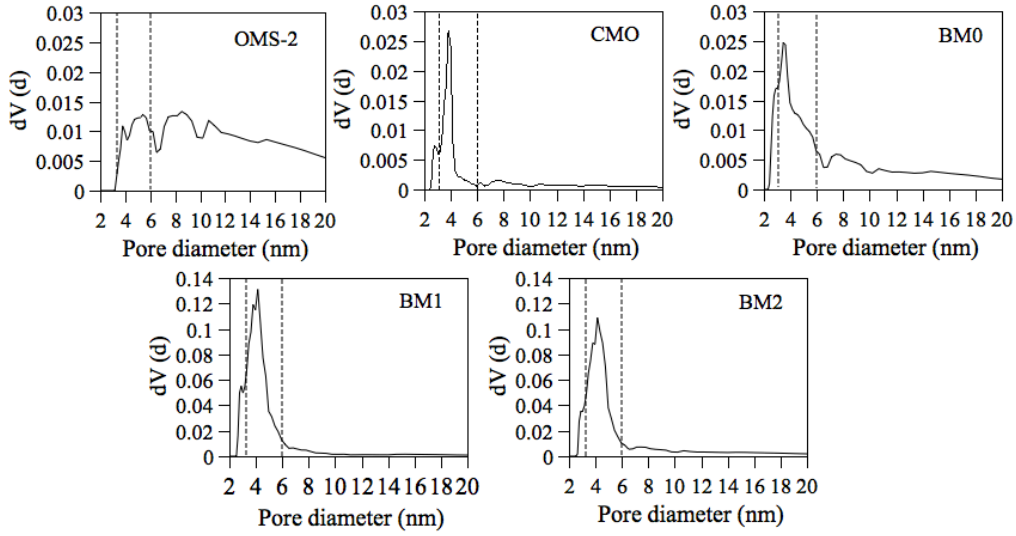

Figure S3. Pore size distribution of catalysts based on NLDFT model. The data fitting errors are within 2%.

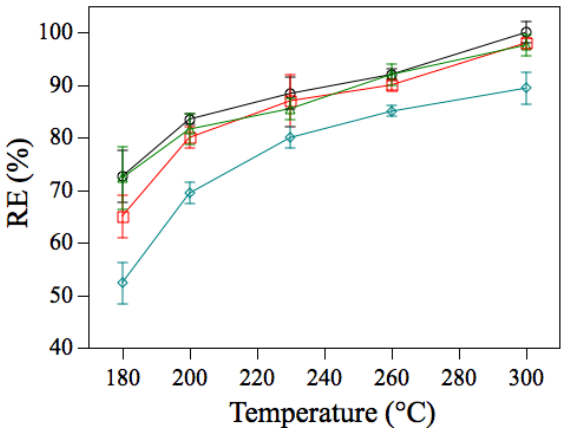

Figure S4. Comparison of catalytic performance of CMO (diamond), BM0 (circle), $BM0_K$ (triangle), and $BM0_{Zr}$ (rectangle).

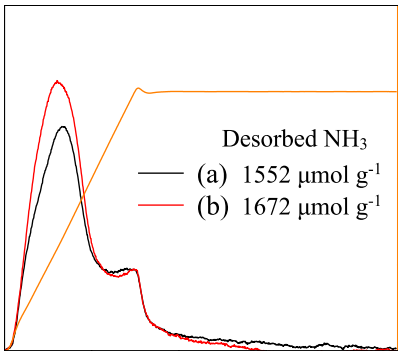

Figure S5. NH_3-TPD profiles of BM2 samples that were subjected to different pretreatment before NH_3 adsorption. (a) BM2 was purged with 60 mL min^{-1} 10% O_2/N_2 at 180 °C for 1 h. (b) BM2 was purged with 60 mL min^{-1} N_2 at 180 °C for 1 h. (c) BM2 was collected after 10.5 h HCBz adsorption in N_2 at 180 °C (d) BM2 was collected after 10.5 h HCBz destruction in 10% O_2 /N_2 at 180 °C.

In order to investigate the impact of atmosphere or reaction on the surface characteristics of catalyst, NH_3-TPD analyses were conducted. Theoretically, the release of surface oxygen species creates oxygen vacancies, which also means the exposure of unsaturated coordinated cation metal centers. These cation centers act as Lewis acid sites, which is responsible for NH_3 adsorption.[5, 6] Therefore, the variation of surface oxygen vacancies can be reflected by the change of NH_3-TPD pattern.

BM2 catalyst was pretreated by various procedures, and then was subjected to NH_3 adsorption, followed by desorption at raising temperature. The desorbed NH_3 was monitored by TCD detector. The total amount of desorbed NH_3 is quantified by integrating the area beneath the NH_3-TPD curve. The NH_3-TPD patterns of BM2 pre-treated in 10%/N_2 or N_2 (Figure S5 a vs. b) involve two peaks: a large peak at 250 °C and a small peak at 400 °C, which can be assigned as weak and strong acid sites, represent the weak and strong binding strength between NH_3 and vacancies. It can be found that BM2 pretreated in N_2 can adsorb more NH_3 than that pretreated in 10% O_2/N_2 (Figure S5 a vs b). This is because the evolution of surface oxygen species in N_2 creates more oxygen vacancies for NH_3 adsorption.

If BM2 is characterized after HCBz adsorption in N_2, the amount of desorbed NH_3 decreases while the distribution of acid strength remains (Figure S4 b vs. c). This reveals that the adsorbed HCBz might cover part of the vacancies, but the intrinsic properties of vacancies are barely changed. It can be concluded that HCBz adsorption mechanism is not based on the chemical interaction between HCBz and vacancies. Although part of HCBz (destruction capacity reaches 22 mg g^{-1} as shown in Figure 4 c) was destructed in N_2 atmosphere, the impact of destruction reaction on vacancy properties is insignificant. It is suspected that the destruction of HCBz by O_{ads} occurs before adsorption. Properties of some vacancies might be changed, but the following adsorbed HCBz blocks pore structure or covers the changed vacancies. These sites cannot access to NH_3 molecule. Hence these changes cannot be reflected in TPD profile.

In another case, when 10% O_2 is induced into the system, oxidative destruction becomes the dominant reaction (removal efficiency is shown in Figure S8, destruction capacity increases to 37 mg g^{-1} while adsorption capacity decreases to 1.2 mg g^{-1}). As shown in Figure S5d, the amount of adsorbed NH_3 decreases accompanied with the significant change of acid strength distribution. The results indicate the strong interaction between vacancies and reaction products. Combining with the observations in stability test and surface chloride analyses, the change of vacancy characteristics is probably due to the occupation of vacancies by Cl^- (reaction (9)). The exposure of Cl^- occupied vacancies to NH_3 might forms $Mn(NH_3)_mCl_n$ complex. The increase of strong acidity might be contributed by the deammoniation of $Mn(NH_3)_mCl_n$ at 504-590 K.[7]

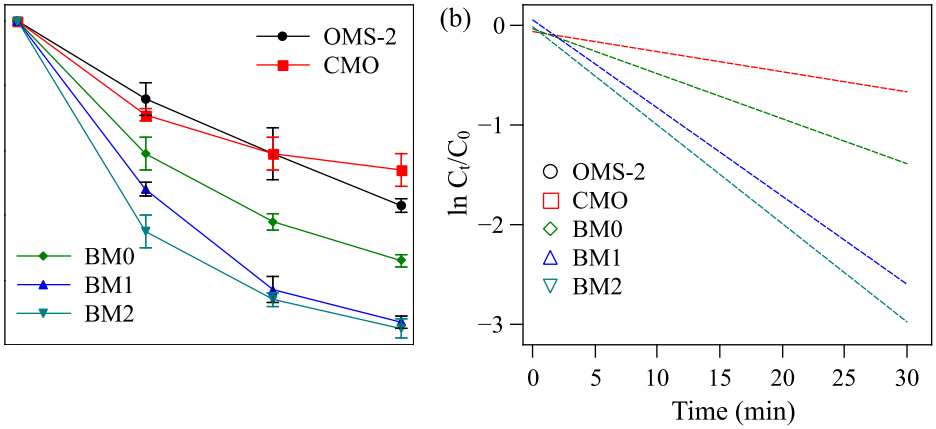

Figure S6. (a) Catalytic destruction of HCBz in batch mode and (b) Fitting of batch reaction data by first order kinetic model.

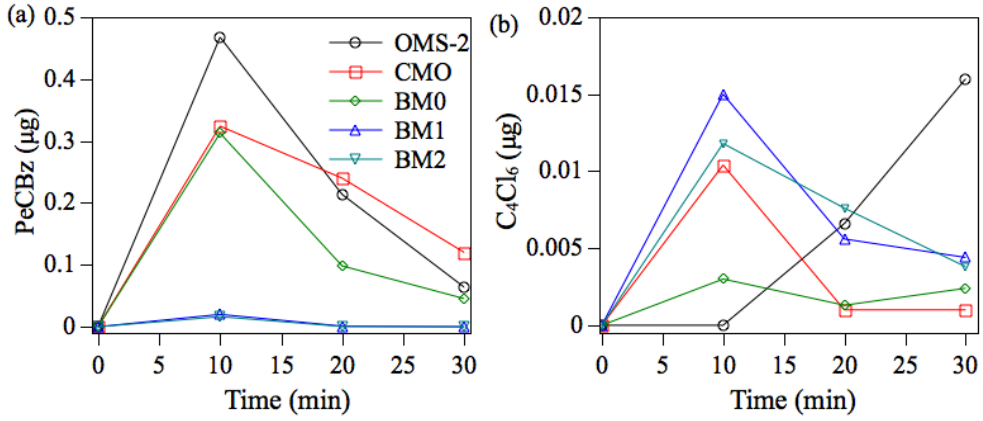

Figure S7. Intermediates concentration as a function of batch reaction time.

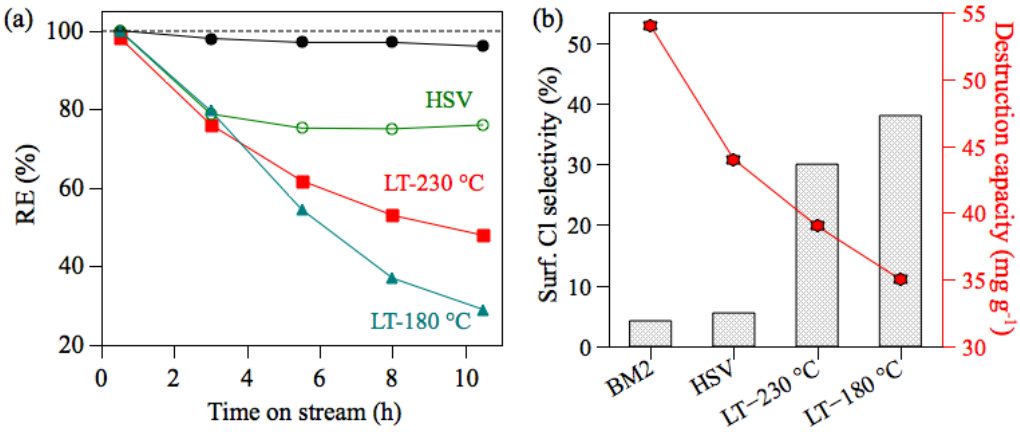

Figure S8. Stability test of BM2 conducted at regular condition (data is cited from Figure 5 and marked in filled cycle), at high space velocity (HSV) scenario (SV of 900000 mL g^{-1} h^{-1}, 300 °C), and at low temperature (LT) scenarios (SV of 450000 mL g^{-1} h^{-1}). In the case of LT-180 °C, 1.2 mg g^{-1} of residual HCBz was found on BM2 after 10.5 h reaction. This value is significantly lower than the adsorption capacities (15 mg g^{-1}, shown in Figure 4c) measured in N_2 atmosphere.

Table S1. Textural properties and elemental composition of catalysts

Catalysts	Surface area	Mesopore volume	Elemental composition		
	(m^2 g^{-1})	(cm^3 g^{-1})	K (wt%)	Mn (wt%)	Fe (wt%)
OMS-2	50	0.29	5.6	58.8	ND*
CMO	40	0.052	ND	61.3	ND
BM0	84	0.16	ND	61.4	1.1
$BM0_{zr}$	88	0.20	ND	62.0	ND
$BM0_K$	74	0.24	0.5	63.0	0.5
BM1	267	0.32	1.2	59.2	0.2
BM2	200	0.30	0.4	56.6	0.3

*ND: not detected

Table S2. Quantification of H_2-TPR and O_2-TPD analyses and TOF calculation.

Catalysts	H_2 consumption (mmol/g)		O_2 desorption (mmol/g)		TOF (10^{-3} s^{-1})
	O_{ads}	Total	O_{ads}	Total	
OMS-2	1.28	8.17	0.96	4.24	11.0
CMO	2.08	8.88	1.20	5.94	9.5
BM0	2.13	7.48	1.79	5.44	18.7
BM1	2.26	5.47	2.38	4.36	18.8
BM2	2.21	5.74	2.85	4.98	19.9

Table S3. Comparison of literature reported activity at 200 °C

Catalysts	HCBz concentration ($mg\ Nm^{-3}$)	Gas flow ($mL\ min^{-1}$)	SV (h^{-1})	DE @ 200 °C (%)	Specific activity ($\mu g\ min^{-1}\ g^{-1}$)	Ref
V_2O_5-WO_3/TiO_2	1 ppm	700	5,000	60	0.625	8
V_2O_5-WO_3/TiO_2	0.01	8000	40,000	32 @ 230 °C	4.67×10^{-5}	9
V_2O_5/TiO_2	70 ppm	37	22,000 [a]	0	0	10
V_2O_5/TiO_2 (CF)[b]	350 ng Nm^{-3}	1.6 m^3/min	NA	95 @ 195 °C	NA	11
V_2O_5-WO_3/TiO_2	7.6	220	660,000 h^{-1}	19 @ 300 °C	15.9	12
δ-MnO_2	7.6	220	660,000 h^{-1}	50	41.8	12
Cu-OMS	7.6	220	660,000 h^{-1}	78	65.2	13
BM2	5.5	300	450,000 mL g^{-1} h^{-1}	100	82.5	This study

[a] Catalyst density was assumed to be 1 mL g^{-1} according to our experience.

[b] CF: Catalytic filter

Literature Cited

1. Shen, X. F.; Ding, Y. S.; Liu, J.; Cai, J.; Laubernds, K.; Zerger, R. P.; Vasiliev, A.; Aindow, M.; Suib, S. L., Control of nanometer- scale tunnel sizes of porous manganese oxide octahedral molecular sieve nanomaterials. *Adv. Mater.* **2005**, *17* (7), 805-809.
2. Ravikovitch, P. I.; Neimark, A. V., Characterization of micro-and mesoporosity in SBA-15 materials from adsorption data by the NLDFT method. *J. Phys. Chem. B* **2001**, *105* (29), 6817-6823.
3. Wang, R. H.; Li, J. H., Effects of precursor and sulfation on OMS-2 catalyst for oxidation of ethanol and acetaldehyde at low temperatures. *Environ. Sci. Tech.* **2010**, *44* (11), 4282-4287.
4. King'ondu, C. K.; Opembe, N.; Chen, C.-h.; Ngala, K.; Huang, H.; Iyer, A.; Garcés, H. F.; Suib, S. L., Manganese oxide octahedral molecular sieves (OMS-2) multiple framework substitutions: a new route to oms-2 particle size and morphology control. *Adv. Funct. Mater.* **2011**, *21* (2), 312-323.
5. Auroux, A.; Gervasini, A., Microcalorimetric study of the acidity and basicity of metal oxide surfaces. *J. Phys. Chem.* **1990**, *94* (16), 6371-6379.
6. Qi, G.; Yang, R. T., Characterization and FTIR studies of MnO_x-CeO_2 catalyst for low-temperature selective catalytic reduction of NO with NH_3. *J. Phys. Chem. B* **2004**, *108* (40), 15738-15747.
7. Reardon, H.; Hanlon, J. M.; Grant, M.; Fullbrook, I.; Gregory, D. H., Ammonia uptake and release in the MnX_2-NH_3 (X = Cl, Br) systems and structure of the Mn $(NH_3)_nX_2$ (n= 6, 2) Ammines. *Crystals* **2012**, *2* (2), 193-212.
8. Weber, R.; Sakurai, T.; Hagenmaier, H., Low temperature decomposition of PCDD/PCDF, chlorobenzenes and PAHs by TiO_2-based V_2O_5-WO_3 catalysts. *Appl. Catal. B: Environ.* **1999**, *20* (4), 249-256.
9. Liljelind, P.; Unsworth, J.; Maaskant, O.; Marklund, S., Removal of dioxins and related aromatic hydrocarbons from flue gas streams by adsorption and catalytic destruction. *Chemosphere* **2001**, *42* (5-7), 615-623.
10. Lee, J. E.; Jurng, J., Catalytic conversions of polychlorinated benzenes and

dioxins with low-chlorine using V_2O_5/TiO_2. *Catal. Lett.* **2008**, *120* (3-4), 294-298.

11. Hung, P. C.; Chang, S. H.; Chang, M. B., Removal of chlorinated aromatic organic compounds from MWI with catalytic filtration. *Aerosol Air Qual. Res.* **2014**, *14*, 1215-1222.
12. Yang, Y.; Huang, J.; Wang, S.; Deng, S.; Wang, B.; Yu, G., Catalytic removal of gaseous unintentional POPs on manganese oxide octahedral molecular sieves. *Appl. Catal. B: Environ.* **2013**, *142–143*, 568-578.
13. Yang, Y.; Huang, J.; Zhang, S.; Wang, S.; Deng, S.; Wang, B.; Yu, G., Catalytic removal of gaseous HCBz on Cu doped OMS: Effect of Cu location on catalytic performance. *Appl. Catal. B: Environ.* **2014**, *150–151*, 167-178.